LETTERS

Solubility trapping in formation water as dominant CO_2 sink in natural gas fields

Stuart M. V. Gilfillan[1,2], Barbara Sherwood Lollar[3], Greg Holland[1], Dave Blagburn[1], Scott Stevens[4], Martin Schoell[5], Martin Cassidy[6], Zhenju Ding[1,7], Zheng Zhou[1], Georges Lacrampe-Couloume[3] & Chris J. Ballentine[1]

Injecting CO_2 into deep geological strata is proposed as a safe and economically favourable means of storing CO_2 captured from industrial point sources[1–3]. It is difficult, however, to assess the long-term consequences of CO_2 flooding in the subsurface from decadal observations of existing disposal sites[1,2]. Both the site design and long-term safety modelling critically depend on how and where CO_2 will be stored in the site over its lifetime[2–4]. Within a geological storage site, the injected CO_2 can dissolve in solution or precipitate as carbonate minerals. Here we identify and quantify the principal mechanism of CO_2 fluid phase removal in nine natural gas fields in North America, China and Europe, using noble gas and carbon isotope tracers. The natural gas fields investigated in our study are dominated by a CO_2 phase and provide a natural analogue for assessing the geological storage of anthropogenic CO_2 over millennial timescales[1,2,5,6]. We find that in seven gas fields with siliciclastic or carbonate-dominated reservoir lithologies, dissolution in formation water at a pH of 5–5.8 is the sole major sink for CO_2. In two fields with siliciclastic reservoir lithologies, some CO_2 loss through precipitation as carbonate minerals cannot be ruled out, but can account for a maximum of 18 per cent of the loss of emplaced CO_2. In view of our findings that geological mineral fixation is a minor CO_2 trapping mechanism in natural gas fields, we suggest that long-term anthropogenic CO_2 storage models in similar geological systems should focus on the potential mobility of CO_2 dissolved in water.

Noble gas and CO_2 carbon isotopes are powerful tracers of crustal fluid processes that act on subsurface CO_2 (refs 5, 7–10). Within a geological storage site, CO_2 injected as a free CO_2 phase (gas or supercritical) may over time be dissolved in solution (solubility trapping), or locked within carbonate minerals by precipitation (mineral trapping)[4,11]. By using noble gas and carbon isotope tracers together to study naturally occurring CO_2 systems, we can uniquely identify and quantify the principal mechanism of the CO_2 phase removal (mineral or solubility trapping) over a timescale not accessible through extant injection studies.

We combine noble gas data from five natural CO_2 reservoirs located within the Colorado Plateau and Rocky Mountain provinces (McCallum dome, Sheep Mountain and McElmo dome, in Colorado; Bravo dome, in New Mexico; and St Johns dome, in Arizona and New Mexico)[7] with new $\delta^{13}C(CO_2)$ isotope data (Table 1). Previous work has shown that noble gas patterns in these gas fields are explained by the stripping of CO_2 gas from the formation water during reservoir filling, followed by partial dissolution of noble gases back into the formation water[7]. We also consider published noble gas and stable isotope information in a further four CO_2-rich natural gas fields (the JM-Brown Bassett (JMBB) field in the Permian basin, Texas[5]; the Kismarja field in the Pannonian basin, Hungary[8]; and the Jilin field in the Songliao basin, Jilin Province, and the Subei basin field, Jiangsu Province, in China[12,13]).

$CO_2/^3He$ ratios within the magmatic range of $(1–10) \times 10^9$ have been used to identify a primary magmatic origin of the CO_2 contained within five natural CO_2 reservoirs of the Colorado Plateau and Rocky Mountain provinces[7]. $CO_2/^3He$ ratios within the Subei basin and the JMBB field also indicate a magmatic origin, but the $CO_2/^3He$ ratios within the Jilin and Kismarja fields are much higher, suggesting a predominantly crustal origin[5,8,12,13]. All of the reservoirs exhibit local variation in the CO_2 content relative to the inert tracer ^3He. As there is not a significant source of ^3He within the crust[14], and as ^3He is inert and highly insoluble[9], this variation must be due to changes in the CO_2 component within the reservoirs. Although many sources and sinks of CO_2 exist in the subsurface[4,8,9], below we argue that the variation in $CO_2/^3He$ ratios is caused by CO_2 loss from the reservoir. The difference between the highest $CO_2/^3He$ ratio and lower values can provide a minimum estimate of this CO_2 loss. In the case of Bravo dome, a reduction in $CO_2/^3He$ values from 4.82×10^9 (well BD11) to 2.25×10^9 (BD02) indicates a loss of the original CO_2 charge of >50% in the portion of the reservoir represented by BD02 (Table 1). Samples from McElmo dome show a decrease from 8.5×10^9 (YD-1) to 0.68×10^9 (HE-2), suggesting a loss of emplaced CO_2 of >90% in portions of this field.

^4He is continually produced in the subsurface by the radiogenic decay of U, Th and K (ref. 14). ^{20}Ne is introduced into the subsurface as a component of air dissolved in water and, as such, can only enter the reservoir system through interaction with formation water[9]. Although there is no *a priori* reason to expect a correlation between ^4He and ^{20}Ne, one has been observed in natural gases on a regional scale[15]. This correlation is the result of ^4He accumulating in the formation water[16], which also contains atmosphere-derived ^{20}Ne, and subsequent quantitative partitioning of both ^4He and ^{20}Ne into the reservoir phase[7,15]. Almost all CO_2 reservoirs for which we have ^{20}Ne and ^4He concentration data show a local ^{20}Ne correlation with ^4He (Table 1 and Supplementary Information). A decrease in $CO_2/^3He$ is also correlated with ^{20}Ne in most CO_2 reservoirs (Fig. 1) and with ^4He in all CO_2 reservoirs (Fig. 2).

There are various mechanisms by which crustal CO_2 ($CO_2/^3He > 10^{10}$) can be added to these systems[4,10], but there is no plausible mechanism that enables crustal CO_2 to be variably added to these systems while preserving a correlation of $CO_2/^3He$ with the noble gases derived from formation water. Neglecting small amounts of ^3He dissolution back into the formation water[7], changes in

[1]School of Earth, Atmospheric and Environmental Sciences, The University of Manchester, Oxford Road, Manchester M13 9PL, UK. [2]Scottish Centre for Carbon Storage, School of GeoSciences, The University of Edinburgh, Grant Institute, Kings Buildings, West Mains Road, Edinburgh EH9 3JW, UK. [3]Department of Geology, University of Toronto, 22 Russell Street, Toronto, Ontario M5S 3B1, Canada. [4]Advanced Resources International, 4501 Fairfax Drive, Suite 910, Arlington, Virginia 22203-1661, USA. [5]GasConsult International, 2808 Adeline Street #3, Berkeley, California 94703, USA. [6]Department of Earth and Atmospheric Sciences, University of Houston, Houston, Texas 77204-5503, USA. [7]China University of Geosciences, Wuhan City, 430074, China.

Table 1 | Sample location, producing formation, major gas species and CO_2 carbon isotopes

Field and well	Location	Producing formation	$CO_2/^3He$ (10^9)	$^3He/^4He$ (R/R_a)	^4He (10^{-4} cm^3 (STP) cm^{-3})	^{20}Ne (10^{-8} cm^3 (STP) cm^{-3})	$\delta^{13}C(CO_2)$ (‰)
Bravo dome[7]							
BD01	35.8613, −103.2947	Tubb	4.53 (10)	1.670 (8)	0.944 (12)	0.169 (2)	−3.96 (4)
BD02	36.0058, −103.2305	Tubb	2.25 (5)	0.764 (4)	4.15 (5)	0.700 (7)	−4.93 (8)
BD03	36.0934, −103.2662	Tubb	2.41 (5)	0.896 (4)	3.31 (4)	0.521 (5)	−4.89 (19)
BD04	35.9766, −103.3480	Tubb	4.61 (10)	1.611 (8)	0.961 (2)	0.181 (2)	−4.23 (8)
BD05	35.9190, −103.2059	Tubb	2.74 (6)	0.965 (5)	2.70 (4)	0.446 (4)	−4.95 (5)
BD06	36.1080, −103.4988	Tubb	3.94 (8)	1.503 (8)	1.20 (2)	0.202 (2)	−4.55 (11)
BD07	35.9046, −103.4190	Tubb	4.34 (9)	2.104 (11)	0.781 (10)	0.180 (2)	−4.85 (1)
BD08	35.8037, −103.4368	Tubb	3.87 (8)	1.143 (6)	1.61 (2)	0.264 (3)	−3.88 (8)
BD09	36.0496, −103.4452	Tubb	4.22 (9)	1.724 (9)	0.981 (12)	0.180 (2)	−4.44 (11)
BD10	36.1519, −103.3557	Tubb	3.25 (6)	1.104 (6)	1.99 (3)	0.308 (3)	−4.88 (7)
BD11	35.8469, −103.7032	Tubb	4.82 (10)	3.784 (19)	0.391 (5)	0.103 (1)	−3.66 (29)
BD12	35.8469, −103.7387	Tubb	4.74 (10)	3.627 (18)	0.415 (6)	NM	−3.94 (17)
BD13	35.7749, −103.2059	Tubb	3.54 (8)	1.318 (7)	1.53 (2)	0.240 (3)	−4.42 (3)
BD14	35.7893, −103.3302	Tubb	4.39 (9)	1.413 (7)	1.15 (2)	0.179 (4)	−4.04 (2)
BD12b	35.8469, −103.7387	Tubb	4.75 (10)	3.634 (18)	0.413 (6)	0.120 (2)	−3.94 (17)
McCallum dome[7]							
No. 3 (8-3)	40.7632, −106.1717	Lakota	1.52 (4)	0.354 (7)	12.3 (2)	1.17 (2)	−5.1 (3)
No. 5	40.7777, −106.2479	Lakota	1.04 (3)	0.409 (7)	15.5 (2)	2.71 (3)	−5.2 (1)
No. 13	40.7777, −106.2289	Lakota/Morrison	0.89 (2)	0.393 (7)	18.8 (2)	4.36 (5)	−5.3 (2)
No. 79	40.7777, −106.2670	Dakota/Lakota	1.77 (6)	0.406 (6)	9.16 (21)	2.53 (3)	−5.7 (1)
McElmo dome[7]							
MC-1	37.4155, −108.7713	Leadville	5.04 (11)	0.145 (2)	9.58 (8)	0.376 (4)	−4.26 (10)
HE-2	37.5052, −108.9094	Leadville	0.68 (15)	0.148 (1)	70.5 (7)	0.307 (30)	−4.40 (10)
YC-4	37.4529, −108.8583	Leadville	4.96 (11)	0.137 (3)	10.2 (10)	0.573 (6)	−4.41 (10)
SC-9	37.3934, −108.8733	Leadville	3.17 (7)	0.150 (3)	14.8 (14)	0.497 (5)	−4.29 (10)
YB-2	37.4472, −108.8075	Leadville	8.74 (20)	0.125 (1)	6.42 (61)	0.371 (4)	−4.40 (10)
YC-1	37.4529, −108.8583	Leadville	4.07 (9)	0.142 (2)	12.1 (12)	0.423 (5)	−4.34 (10)
HF-1	37.4871, −108.8807	Leadville	2.16 (6)	0.169 (1)	19.3 (26)	0.564 (12)	−4.37 (10)
HD-2	37.4572, −108.9008	Leadville	4.28 (10)	0.140 (3)	11.7 (12)	0.128 (2)	−4.38 (10)
YA-2	37.4692, −108.7811	Leadville	3.39 (8)	0.138 (3)	15.0 (15)	0.130 (2)	−4.42 (10)
YE-1	37.4818, −108.8123	Leadville	4.16 (9)	0.173 (3)	9.75 (8)	0.143 (3)	−4.45 (10)
HA-1	37.5289, −108.8718	Leadville	4.56 (10)	0.139 (3)	11.0 (11)	0.205 (7)	−4.66 (10)
SC-10	37.3934, −108.8733	Leadville	4.37 (10)	0.139 (2)	11.6 (11)	0.413 (5)	−4.27 (10)
HC-2	37.4734, −108.8860	Leadville	4.68 (11)	0.140 (2)	10.7 (10)	0.409 (5)	−4.38 (10)
HB-1	37.5087, −108.8802	Leadville	4.74 (11)	0.148 (3)	9.94 (10)	0.247 (4)	−4.49 (10)
YD-1	37.4619, −108.8224	Leadville	8.50 (20)	0.145 (3)	5.68 (6)	0.366 (5)	−4.46 (10)
JM-Brown Basset field[5]							
Turk State No. 1A	30.38758, −101.85642	Ellenberger	5.92 (47)	0.543 (16)	1.25 (9)	NM	−2.88 (3)
Bassett Goode No. 3	30.37852, −101.83068	Ellenberger	5.55 (43)	0.527 (16)	1.42 (10)	NM	−2.89 (3)
Brown Bassett No. 2*	30.34433, −101.7995	Ellenberger	5.82 (35)	0.502 (15)	1.33 (7)	NM	−2.90 (3)
Mayme K. Martin ETAL 1	30.35661, −101.74721	Ellenberger	5.29 (40)	0.372 (11)	1.42 (10)	NM	−2.97 (3)
Mitchell 109 No. 2*	30.33329, −101.69826	Ellenberger	4.58 (36)	0.400 (12)	1.53 (11)	NM	−2.92 (3)
Mitchell 5 No. 1X	30.32352, −101.68429	Ellenberger	5.61 (43)	0.478 (11)	1.40(10)	NM	−2.84 (3)
Mitchell 103 No. 2	30.3568, −101.63642	Ellenberger	4.20 (33)	0.246 (7)	1.39 (10)	NM	−2.70 (3)
Mitchell No. 6	30.351, −101.58835	Ellenberger	3.93 (31)	0.264 (8)	1.51 (11)	NM	−2.96 (3)
Mitchell No. 3	30.33966, −101.61307	Ellenberger	4.22 (33)	0.240 (7)	1.39 (10)	NM	−3.06 (3)
Mitchell A-11 No. 1	30.30286, −101.57677	Ellenberger	4.07 (32)	0.272 (8)	1.66 (12)	NM	−2.93 (3)
Mitchell No. 12	30.29118, −101.57295	Ellenberger	4.24 (130)	0.267 (8)	1.46 (10)	NM	−2.96 (3)
Sheep Mountain[7]							
8-2-P	37.6383, −105.1836	Dakota	2.31 (5)	0.981 (10)	3.13 (3)	1.47 (2)	−5.0 (2)
2-10-O	37.6966, −105.2018	Entrada	2.44 (6)	0.984 (12)	2.96 (3)	3.04 (3)	−5.2 (1)
9-26	37.6675, −105.1836	Dakota	2.57 (6)	0.934 (14)	2.95 (3)	0.613 (9)	NM
2-9-H	37.7112, −105.2200	Dakota	2.44 (6)	0.945 (19)	3.07 (3)	9.77 (10)	NM
3-15-B	37.6966, −105.2018	Dakota	2.61 (6)	0.937 (16)	2.90 (3)	1.54 (2)	−5.7 (4)
4-13	—	Dakota	2.17 (5)	0.942 (18)	3.47 (4)	1.11 (2)	NM
4-26-E	37.6675, −105.1836	Entrada	2.20 (5)	1.024 (18)	3.15 (3)	0.442 (4)	−4.8 (1)
3-23-D	37.6820, −105.2018	Dakota	2.26 (5)	0.988 (14)	3.17 (3)	0.579 (9)	NM
7-35-L	37.6383, −105.1836	Dakota	2.53 (6)	0.916 (14)	3.06 (3)	0.749 (12)	−5.0 (2)
2-35-C	37.6675, −105.1836	Dakota	2.57 (6)	0.963 (19)	2.87 (3)	0.573 (8)	NM
1-15-C	37.6966, −105.2018	Entrada	2.71 (6)	0.967 (16)	2.71 (3)	6.77 (10)	NM
3-4-O	37.7112, −105.2200	Dakota	2.53 (6)	0.937 (14)	2.99 (3)	2.64 (3)	−5.8 (3)
4-14-M	37.6820, −105.2018	Dakota	2.65 (6)	0.892 (15)	3.00 (3)	1.11 (1)	NM
5-15-O	37.6820, −105.2018	Dakota	2.30 (5)	1.056 (15)	2.92 (3)	4.33 (5)	−5.0 (1)
4-4-P	37.7112, −105.2200	Dakota	2.90 (7)	0.970 (14)	2.52 (2)	1.31 (2)	NM
5-9-A	37.7112, −105.2200	Dakota	2.39 (6)	1.006 (18)	2.94 (3)	1.28 (2)	NM
1-1-J	37.6383, −105.1836	Dakota	3.61 (8)	0.908 (16)	2.16 (2)	0.878 (12)	−5.2 (1)
1-22-H	37.5946, −105.2018	Entrada	2.25 (5)	0.981 (17)	3.22 (3)	0.937 (13)	−4.5 (2)
St Johns dome[7]							
22-1X	34.4265, −109.2664	Supai	0.098 (2)	0.455 (8)	134 (13)	34.4 (47)	−3.65 (5)
10-22	34.2437, −109.1645	Supai	1.91 (42)	0.394 (8)	9.42 (9)	2.30 (4)	−3.79 (5)
3-1	34.3771, −109.2563	Supai	0.22 (3)	0.433 (9)	70.6 (7)	15.1 (21)	−3.85 (5)
Jilin field[12,13,21]							
Wan 2	—	Cretaceous	1.44 (4)	4.91 (6)	1.00 (2)	NM	−3.6
Wan 5	—	Cretaceous	227 (7)	4.10 (4)	0.0076 (2)	0.0547 (15)	−5.0
Wan 6	—	Cretaceous	8.32 (3)	4.99 (5)	0.169 (4)	0.230 (6)	−3.8
Wan 8	—	Cretaceous	NM	4.30 (5)	NM	NM	−3.2

Table 1 is continued on page 616.

Table 1 | Continued

Field and well	Location	Producing formation	$CO_2/^3He$ (10^9)	$^3He/^4He$ (R/R_a)	^4He (10^{-4} cm^3 (STP) cm^{-3})	^{20}Ne (10^{-8} cm^3 (STP) cm^{-3})	$\delta^{13}C(CO_2)$ (‰)
Wan 9	—	Cretaceous	36.6 (10)	4.08 (4)	0.047 (1)	0.130 (3)	−3.8
Subei field[12,21]							
Huangqian 1	—	Permian	2.17 (7)	3.52 (5)	3.13 (3)	1.47 (2)	−3.6
Sutail 74	—	Devonian	0.493(14)	3.59 (4)	2.96 (3)	3.04 (3)	−4.1
Su203	—	Eocene	0.459 (13)	2.61 (3)	2.95 (3)	0.613 (9)	−2.7
Kismarja field[8,29]							
Kismarja 8	—	Up. Pannonian	20.2 (5)	1.33 (3)	0.226 (7)	NM	−5.0
Kismarja 79	—	Up. Pannonian	15.5 (4)	1.38 (3)	0.310 (10)	NM	−4.9
Kismarja 61	—	Up. Pannonian	27.3 (6)	1.16 (2)	0.205 (6)	NM	−5.1
Kismarja 55	—	Up. Pannonian	13.3 (3)	1.38 (3)	0.360 (11)	NM	−5.1
Kismarja 56	—	Up. Pannonian	1090 (3)	1.16 (2)	0.0052 (2)	NM	−6.8
Kismarja 74	—	Up. Pannonian	65.2 (2)	1.34 (3)	0.078 (3)	NM	−6.4
Kismarja 22	—	Up. Pannonian	1.52 (1)	1.02 (2)	1.31 (3)	NM	−6.6

Location is given as latitude and longitude in decimal degress, where north and east are positive and south and west are negative. The $^3He/^4He$ ratio, R, is shown relative to the $^3He/^4He$ ratio in air, R_a, which is taken to be 1.399×10^{-6}. $\delta^{13}C‰ = [(^{13}C/^{12}C_{sample} - {}^{13}C/^{12}C_{standard})/(^{13}C/^{12}C_{standard})] \times 1{,}000$; the standard used is the Vienna PeeDee Belemnite. Errors (1σ) are shown in parentheses. NM, not measured.
* Average of two analyses for He and Ar.

$CO_2/^3He$ must therefore be due to CO_2 loss in the subsurface by an amount directly proportional to the amount of formation water that has been degassed. CO_2 is soluble and reactive. The most probable mechanisms of subsurface CO_2 fluid phase removal are solubility and/or mineral trapping[4,11].

Reservoir lithology may exert a significant influence on how changes in $CO_2/^3He$ ratio relate to $\delta^{13}C(CO_2)$. The carbonate reservoirs (the JMBB field and the McElmo and St Johns domes) show little variance in $\delta^{13}C(CO_2)$, whereas the siliciclastic fields (the Jilin, Subei basin and Kismarja fields, Sheep Mountain, McCallum dome and Bravo dome) exhibit a greater $\delta^{13}C(CO_2)$ range (Table 1 and Supplementary Fig. 1). We consider Bravo dome and McElmo dome as representative cases for each type of reservoir lithology.

Emplacement of CO_2 at Bravo dome is believed to have occurred relatively recently (local volcanic activity dates from 8,000 to 10,000 years ago)[7,17], and the field may still be undergoing active CO_2 recharge[11]. The decreasing $CO_2/^3He$ ratio within Bravo dome correlates with more negative $\delta^{13}C(CO_2)$ (Fig. 3a). Taking the highest $CO_2/^3He$ ratio, of 4.82×10^9 (BD11), to be the sample that experienced

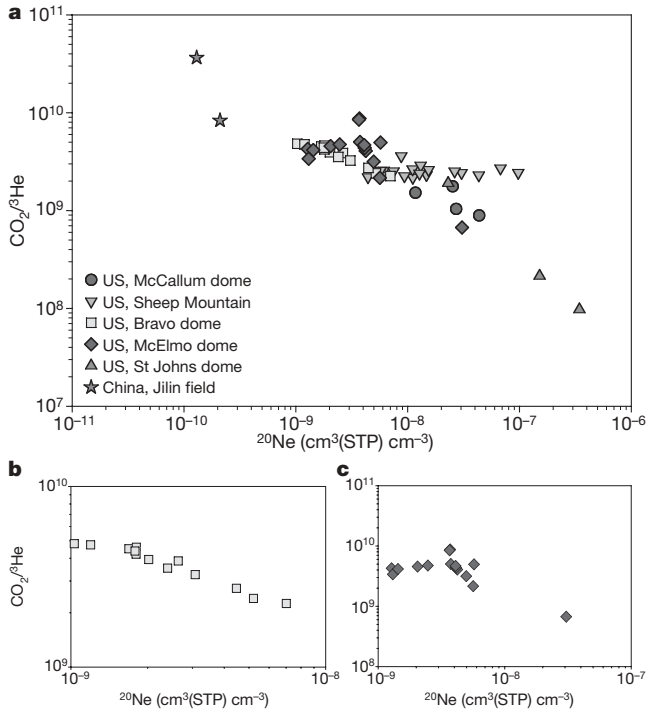

Figure 1 | $CO_2/^3He$ variation plotted against ^{20}Ne from CO_2-rich natural gas fields. **a**, There is a general trend in this data set of decreasing $CO_2/^3He$ with increasing ^{20}Ne. **b**, **c**, This trend is most clear in the siliciclastic-case data set, from Bravo dome (**b**), but less clear in the data from the carbonate-case reservoir, McElmo dome (**c**). ^3He is conservative within the gas phase. Lower $CO_2/^3He$ ratios therefore represent subsurface reduction in CO_2 concentration in the emplaced CO_2 phase. Because the only subsurface source of the ^{20}Ne is the formation water, the CO_2 sink must be linked to the formation water contacted by the gas phase. STP indicates measurement at the International Union of Pure and Applied Chemistry (IUPAC) standard temperature (0 °C) and pressure (100 kPa).

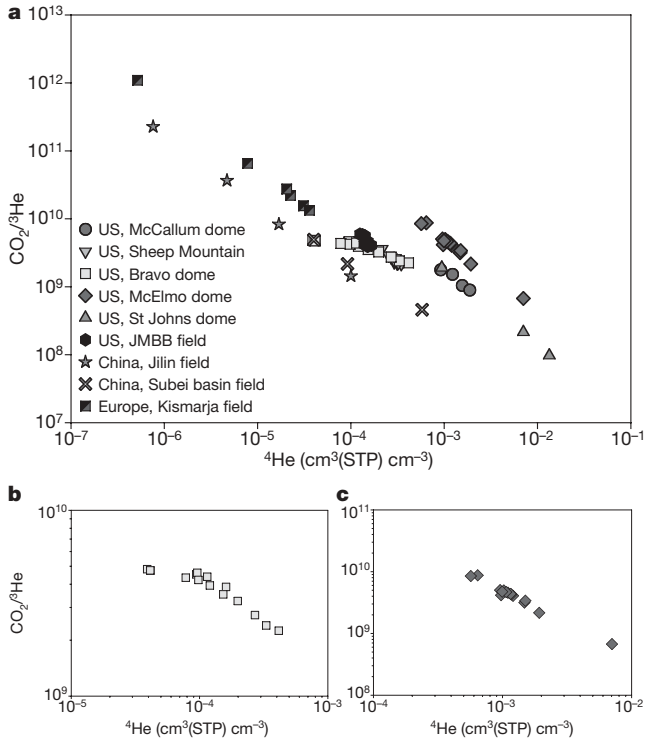

Figure 2 | $CO_2/^3He$ in CO_2-rich natural gas fields shows strong anticorrelation with ^4He. **a**, ^4He accumulates in formation water over time[7,15,16] and underscores the importance of formation water in controlling the mechanism of subsurface CO_2 removal (Fig. 1 and main text). We speculate that the formation-water ^4He signature with $CO_2/^3He$ is more coherent than the equivalent ^{20}Ne signature (Fig. 1) owing to perturbation of ^{20}Ne in ancient formation water through non-water phase interaction[9], with subsequent ^4He accumulation providing a homogenous, regional-scale formation-water ^4He signal[15,16]. Different $CO_2/^3He$-versus-^4He gradients are due to different local formation-water ^4He accumulation rates. **b**, **c**, As in Fig. 1, but for ^4He.

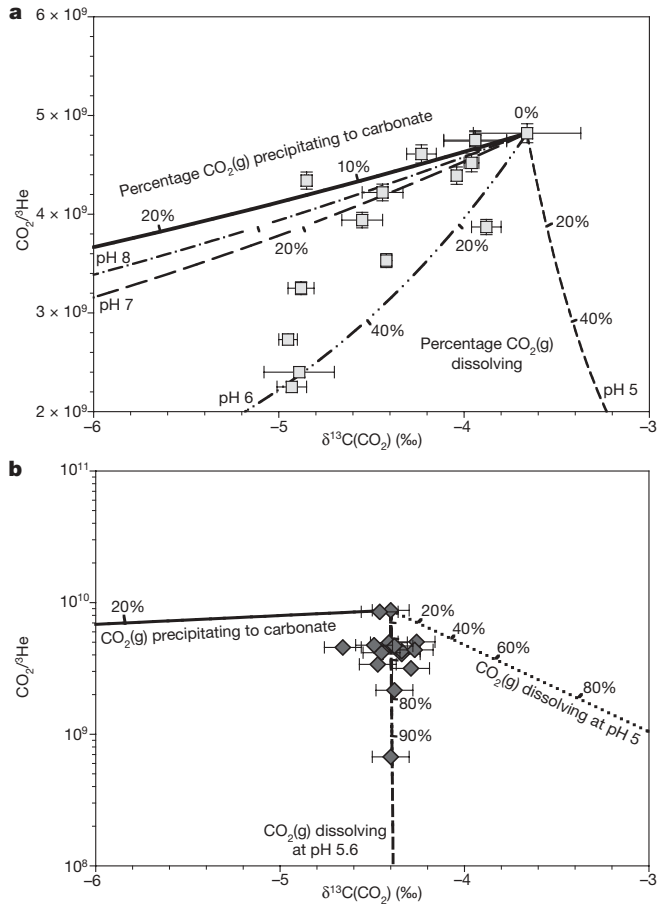

Figure 3 | Plot of $\delta^{13}C(CO_2)$ against $CO_2/^3He$ for Bravo dome and McElmo dome. **a**, Bravo Dome. The solid line shows the predicted trend for carbonate mineral precipitation and the broken lines show CO_2(g) dissolution trends for the indicated formation-water pH (see Methods Summary). This data limits the maximum effect of CO_2 precipitation in samples to approximately 18%. **b**, McElmo Dome. Invariant $\delta^{13}C(CO_2)$ with a change in $CO_2/^3He$ of over an order of magnitude in McElmo dome gases cannot be accounted for by precipitation (solid line). Dissolution of reservoir CO_2 into formation water at pH 5.6 is consistent with observed results. Error bars are 1σ.

the least CO_2 loss, we calculate the coherent change in $CO_2/^3He$ and $\delta^{13}C(CO_2)$ predicted for CO_2 dissolution into the formation water at various pH values and for CO_2 precipitation as a carbonate (Methods Summary). The data are not consistent with precipitation as carbonate being a major sink for CO_2 at Bravo dome (Fig. 3a). However, although a significant number of the data points are consistent with CO_2 dissolution into formation water at a pH between 6 and 7, it is not possible to rule out a degree of CO_2 loss due to precipitation together with CO_2 dissolution at a lower pH (for example pH 5). In such a two-process model, an upper limit of approximately 18% can be set on the proportion of CO_2 lost to precipitation (Fig. 3a). Hence, in all cases the major CO_2 sink is dissolution.

In situ precipitation of 18% of reservoir CO_2 would generate between 3.2 and 6.1% by mass of the whole rock, depending on whether dolomite, calcite or dawsonite precipitation was favoured by the reservoir conditions. Although evidence for CO_2-rich formation water interaction within the reservoir has been documented, so far no secondary carbonate has been identified[18]. Nevertheless, the volume control of the water suggests that the location of the precipitate, if any, is likely to be within the water leg that was not sampled. Lack of reservoir secondary mineralization cannot at this stage rule out any carbonate precipitation as a minor CO_2 sink.

Similar to the case for Bravo dome, although many of the Sheep Mountain data can be accounted for by dissolution of CO_2 (at pH 5 in this case), a small component of precipitation cannot be ruled out. Adopting the same approach as used for Bravo dome, we find that the remaining Sheep Mountain data require a maximum of 10% precipitation and 20% dissolution of the original CO_2 charge (Table 1 and Supplementary Fig. 2). By contrast, although minor data scatter may also be due to some small amount of CO_2 precipitation or dissolution at pH 7–8, almost all the data from the other siliciclastic fields (McCallum dome and the Subei basin, Kismarja and Jilin fields) can be described by dissolution into the formation water alone, within a narrow pH range of 5–5.3 (Supplementary Figs 3–6).

Carbonate reservoir data from McElmo dome show a change in $CO_2/^3He$ ratio of over an order of magnitude, with invariant $\delta^{13}C(CO_2)$ (Fig. 3b). This pattern is repeated in the two other carbonate-dominated fields (Supplementary Figs 7, 8). Invariant $\delta^{13}C(CO_2)$ in these fields allows us to discount a two-process model of precipitation and dissolution such as at Bravo dome (Fig. 3a). These data are consistent with CO_2 dissolution only into formation water in the pH range of 5.4–5.8 (Fig. 3b and Supplementary Figs 7, 8), a value similar to the pH obtained for the siliciclastic reservoirs and to values observed (pH 5.7) in carbonate-mineral-buffered formation water observed in the recent CO_2 injection studies on CO_2 breakthrough[19] in the Frio formation, Texas.

On a reservoir-engineering timescale, the early stages of CO_2 injection can result in a drop in pH and dissolution of carbonate minerals into the formation water[18–20,22]. Any significant CO_2 contribution to the reservoir CO_2 phase from re-dissolution of carbonates would be ^3He free and would therefore perturb the correlation between $CO_2/^3He$ ratio and ^4He and ^{20}Ne. As there is a clear correlation between $CO_2/^3He$ ratio and ^4He in all fields and ^{20}Ne within the majority, we conclude that dissolution of carbonate minerals into the formation water cannot have had a major influence on $\delta^{13}C(CO_2)$ values. There is no evidence for any precipitation of CO_2 within the carbonate-dominated reservoirs, requiring that the dominant mechanism of reservoir CO_2 loss, accounting for up to 90%, is through dissolution into the formation water.

Even the most conservative model we have presented places an upper limit of approximately 18% on the CO_2 removed by precipitation, and then only in some samples, from all natural gas fields investigated in a variety of lithological settings. Precipitation of CO_2 over millennial timescales represents at most only a small subsurface trapping mechanism for CO_2, and only within siliciclastic lithologies. The dominant mechanism of CO_2 loss from most CO_2 natural gas fields can be accounted for through simple dissolution into the formation groundwater within a narrow pH window (pH 5–5.8). This study underscores the fact that understanding geological carbon storage requires careful investigation of existing geological and hydrogeological analogues that have naturally accumulated and stored CO_2 over timescales relevant to anthropogenic CO_2 storage facilities. We have also demonstrated a means of testing trapping and storage mechanisms through coupled measurements of noble gas and carbon isotopes in the context of the pH evolution of formation/reservoir water.

METHODS SUMMARY

Detailed descriptions of the sample collection and analysis procedures can be found in the original references[5,7,8,12,13,21]. In our calculations (Fig. 3 and Supplementary Figures) we use the highest $CO_2/^3He$ ratio measured in each field as a reference point to calculate the correlated reservoir $CO_2/^3He$ and $\delta^{13}C(CO_2)$ ratios as the CO_2 phase is removed by either precipitation or dissolution. We assume open system loss. In the case of precipitation there is zero ^3He loss from the CO_2 phase and $CO_2/^3He$ changes in proportion to the fraction of the remaining CO_2 phase. In the case of dissolution, the change in $CO_2/^3He$ ratio is calculated following the Rayleigh equation.

Changes in $\delta^{13}C(CO_2)$ are calculated using the Rayleigh fractionation equation expressed as $\delta^{13}C(CO_2) = \delta^{13}C(CO_2)_o + \varepsilon \ln f$ (ref. 23), where $\delta^{13}C(CO_2)_o$ is the original system value, f is the fraction of CO_2 remaining in the reservoir and ε is the carbon isotope fractionation, either for precipitation or for dissolution. Carbon isotope fractionation factors, α, are calculated as a function of temperature for

CO_2(g) precipitating to form $CaCO_3$(s), or dissolving to form either H_2CO_3(aq) or HCO_3^-(aq) (ref. 24). Because all the fractionations are small, the simplification can be made that $\varepsilon = 1{,}000\ln\alpha$ (ref. 25). For typical reservoir waters of pH 5–8, the contribution of CO_3^{2-}(aq) is negligible. Hence, for CO_2 dissolution, carbon isotope fractionation between the pool of dissolved inorganic carbon (DIC) and CO_2 gas used in the Rayleigh fractionation equation can be expressed as (ref. 23)

$$\varepsilon^{13}C_{DIC-CO_2(g)} = x(\varepsilon^{13}C_{H_2CO_3(aq)-CO_2(g)}) + (1-x)(\varepsilon^{13}C_{HCO_3^-(aq)-CO_2(g)})$$

where x is the proportion of CO_2(g) dissolving to H_2CO_3(aq) at the relevant pH[23].

Solubility as a function of temperature and salinity is given by the IUPAC solubility series for CO_2 (ref. 26) and in refs 27, 28 for He. The average well depth, reservoir pressure, temperature and salinity are presented in the Supplementary Information for each reservoir, with the corresponding Henry's law constants K_{He} and K_{CO_2} and fractionation factor ($1{,}000\ln\alpha$) for CO_2(g) forming H_2CO_3(aq), HCO_3^-(aq) and $CaCO_3$(s) (Supplementary Table 1).

Received 24 June 2008; accepted 22 January 2009.

1. Schrag, D. P. Preparing to capture carbon. *Science* **315,** 812–813 (2007).
2. Baines, S. J. & Worden, R. H. in *Geological Storage of Carbon Dioxide* (eds Baines, S. J. & Worden, R. H.) 1–6 (The Geological Society of London, 2004).
3. Gale, J. in *Geological Storage of Carbon Dioxide* (eds Baines, S. J. & Worden, R. H.) 7–15 (The Geological Society of London, 2004).
4. Bradshaw, J., Boreham, C. & La Pedalina, F. in *Proc. 7th Internat. Conf. Greenhouse Gas Control Technol. (GHGT-7)* (eds Rubin, E., Keith, D. & Gilboy, C.) 541–550 (Elsevier Science, 2004).
5. Ballentine, C. J., Schoell, M., Coleman, D. & Cain, B. A. 300-Myr-old magmatic CO_2 in natural gas reservoirs of the west Texas Permian basin. *Nature* **409,** 327–331 (2001).
6. Kintisch, E. The greening of synfuels. *Science* **320,** 306–308 (2008).
7. Gilfillan, S. M. V. *et al.* The noble gas geochemistry of natural CO_2 gas reservoirs from the Colorado Plateau and Rocky Mountain provinces, USA. *Geochim. Cosmochim. Acta* **72,** 1174–1198 (2008).
8. Sherwood Lollar, B., Ballentine, C. J. & O'Nions, R. K. The fate of mantle-derived carbon in a continental sedimentary basin: Integration of C/He relationships and stable isotope signatures. *Geochim. Cosmochim. Acta* **61,** 2295–2308 (1997).
9. Ballentine, C. J., Burgess, R. & Marty, B. in *Noble Gases in Geochemistry and Cosmochemistry* (eds Porcelli, D. R., Ballentine, C. J. & Weiler, R.) 539–614 (Geochemical Society and Mineralogical Society of America, 2002).
10. Cathles, L. M. & Schoell, M. Modeling CO_2 generation, migration and titration in sedimentary basins. *Geofluids* **7,** 441–450 (2007).
11. Baines, S. J. & Worden, R. H. in *Geological Storage of Carbon Dioxide* (eds Baines, S. J. & Worden, R. H.) 59–85 (The Geological Society of London, 2004).
12. Xu, S., Nakai, S., Wakita, H., Xu, Y. & Wang, X. Carbon isotopes of hydrocarbons and carbon dioxide in natural gases in China. *J. Asian Earth Sci.* **15,** 89–101 (1997).
13. Xu, S., Nakai, S., Wakita, H. & Wang, X. Mantle-derived noble gases in natural gases from Songliao Basin, China. *Geochim. Cosmochim. Acta* **59,** 4675–4683 (1995).
14. Ballentine, C. J. & Burnard, P. G. in *Noble Gases in Geochemistry and Cosmochemistry* (eds Porcelli, D. R., Ballentine, C. J. & Weiler, R.) 481–538 (Geochemical Society and Mineralogical Society of America, 2002).
15. Ballentine, C. J. & Sherwood Lollar, B. Regional groundwater focusing of nitrogen and noble gases into the Hugoton-Panhandle giant gas field, USA. *Geochim. Cosmochim. Acta* **66,** 2483–2497 (2002).
16. Torgersen, T. & Clarke, W. B. Helium accumulation in groundwater. I: An evaluation of sources and the continental flux of crustal ^{4}He in the Great Artesian Basin, Australia. *Geochim. Cosmochim. Acta* **49,** 1211–1218 (1985).
17. Broadhead, R. F. Natural accumulations of carbon dioxide in the New Mexico region - Where are they, how do they occur and what are the uses for CO_2? *Lite Geol.* **20,** 2–6 (1998).
18. Pearce, J. *et al.* Natural occurrences as analogues for the geochemical disposal of carbon dioxide. *Energy Convers. Manage.* **37,** 1123–1128 (1996).
19. Kharaka, Y. K. *et al.* Gas-water-rock interactions in Frio Formation following CO2 injection: Implications for the storage of greenhouse gases in sedimentary basins. *Geology* **34,** 577–580 (2006).
20. Knauss, K. G., Johnson, J. W. & Steefel, C. I. Evaluation of the impact of CO_2, co-contaminant gas, aqueous fluid and reservoir rock interactions on the geologic sequestration of CO_2. *Chem. Geol.* **217,** 339–350 (2005).
21. Xu, S., Shun'ichi, N., Wakita, H., Xu, Y. & Wang, X. Helium isotope compositions in sedimentary basins in China. *Appl. Geochem.* **10,** 643–656 (1995).
22. Worden, R. H. & Smith, L. K. in *Geological Storage of Carbon Dioxide* (eds Baines, S. J. & Worden, R. H.) 211–224 (The Geological Society of London, 2004).
23. Clark, I. D. & Fritz, P. *Environmental Isotopes in Hydrology* 55–61 (CRC, 1997).
24. Deines, P., Langmuir, D. & Harmon, R. S. Stable carbon isotopes and the existence of a gas phase in the evolution of carbonate groundwaters. *Geochim. Cosmochim. Acta* **38,** 1147–1184 (1974).
25. Fritz, P. & Fontes, J. C. *Handbook of Environmental Isotope Geochemistry* Vol. 1, 1–19 (Elsevier, 1980).
26. Scharlin, P. & Cargill, R. W. *Carbon Dioxide in Water and Aqueous Electrolyte Solutions* (Solubility Data Series Vol. 62, IUPAC, 1996).
27. Crovetto, R., Fernandez-Prini, R. & Laura Japas, M. Solubilities of inert gases and methane in H_2O and in D_2O in the temperature range of 300 to 600K. *J. Chem. Phys.* **76,** 1077–1086 (1982).
28. Smith, S. P. Noble gas solubility in water at high temperature. *Eos* **66,** 397 (1985).
29. Sherwood Lollar, B., O'Nions, R. K. & Ballentine, C. J. Helium and neon isotope systematics in carbon dioxide-rich and hydrocarbon-rich gas reservoirs. *Geochim. Cosmochim. Acta* **58,** 5279–5290 (1994).

Supplementary Information is linked to the online version of the paper at www.nature.com/nature.

Acknowledgements S.M.V.G. was supported by a Natural Environmental Research Council (NERC)-funded PhD studentship in Manchester and a NERC-funded postdoctoral position, grant NE/C516479/1 in Edinburgh and Glasgow, and UK Energy Research Centre grant NE/C513169/1. Manchester work was further partly funded by NERC grants NE/D004292 and NE/F002823. Toronto work was further partly funded by an Natural Sciences and Engineering Research Council of Canada Discovery grant to B.S.L. We thank the field operators for permission to sample the US gas reservoirs and support in the field, particularly L. Nugent (Sheep Mountain), T. Muhic and D. Miller and G. Grove (McCallum dome) and T. White (St Johns dome). S.M.V.G. would like to thank R. S. Haszeldine and Z. Shipton for supporting this work. Review by R. H. Worden is appreciated.

Author Contributions S.M.V.G., C.J.B. and B.S.L. designed the study, analysed the samples, interpreted the data and wrote the paper. G.H., D.B., Z.D., Z.Z. and G.L.-C. assisted with sample analysis and interpretation of the data. S.S., M.S. and M.C. assisted with sample collection and provided comments on the manuscript.

Author Information Reprints and permissions information is available at www.nature.com/reprints. Correspondence and requests for materials should be addressed to S.M.V.G. (stuart.gilfillan@ed.ac.uk).